

Analysis of the three-dimensional ordering of epitaxial Ge quantum dots using focused ion beam tomography

Alan J. Kubis^{a)}

Department of Materials Science and Engineering, University of Virginia, Charlottesville, Virginia 22904

Thomas E. Vandervele

Department of Physics, University of Virginia, Charlottesville, Virginia 22904

John C. Bean

Department of Electrical and Computer Engineering, University of Virginia, Charlottesville, Virginia 22904

Derren N. Dunn

IBM Microelectronics, Hopewell Junction, New York 12533

Robert Hull

Department of Materials Science and Engineering, University of Virginia, Charlottesville, Virginia 22904

(Received 5 December 2005; accepted 6 February 2006; published online 26 June 2006)

Buried layers in quantum dot (QD) superlattices influence the position of QDs in the subsequently grown layers through strain field interactions. Since the strain interactions are complex, a three-dimensional reconstruction of the superlattice can enhance the fundamental understanding of self-organization mechanisms. We have studied the three-dimensional relationship of QDs using focused ion beam tomography. Analysis of the reconstruction is consistent with earlier models for self-organization. QDs on successive layers form above buried QDs. In certain cases, successive QDs in a column decrease in size, resulting in the elimination of the column while QDs in other columns grow in size. © 2006 American Institute of Physics. [DOI: 10.1063/1.2217930]

Much work has been done to study the phenomenon of self-assembly in epitaxial quantum dot (QD) systems.¹⁻⁴ In Si/Ge the lattice mismatch between the two materials, Ge having the larger lattice constant by 4.1% at room temperature, causes strain when one is grown on the other. This strain can be relieved through the formation of QDs. If sets of bilayers are then formed by overgrowing each successive layer of QDs with a film of the substrate material a QD superlattice can be formed. Strain fields due to the buried QDs make it favorable for the QDs on subsequent layers to form above the buried QDs, thus forming columns. While the QDs on the initial layer nucleate and grow essentially randomly (with any deliberate externally induced organization mechanism absent) subsequent layers are known to self-organize.⁵ Previously, it has been observed that spatial organization occurs such that the QDs in the later layers deviate from being centered on the lower QDs to positions that more evenly space the quantum dots. The driving force for this is believed to be due to minimization of the system strain energy through QD-QD interaction.⁶⁻⁸ Techniques such as transmission electron microscopy (TEM), scanning tunneling microscopy (STM), and atomic force microscopy (AFM) have been used to analyze these structures. In the case of STM and AFM only the topmost layer can be observed while TEM gives a two-dimensional projection of a three-dimensional volume. Modeling papers that explore the QD ordering phenomenon have thus been only able to draw upon these two-dimensional observations.^{3,4} To gain a greater insight into these self-assembly processes, we have used the focused ion beam (FIB) to tomographically recon-

struct a full three-dimensional representation of the QD superlattice structure.

Ge and Si films were grown via molecular-beam epitaxy (MBE) on (100) Si substrates using a custom built VG 90S double-chamber UHV-MBE system at the University of Virginia.⁹ Details of the growth conditions have been reported previously.¹⁰ The QD superlattice was analyzed by cross-sectional TEM analysis and no dislocations were observed (within the limited field of cross-sectional TEM imaging, only tens of μm^3 of superlattice region sampled), i.e., the QDs remain coherent. This is despite the fact that the QDs are relatively large, with diameters of approximately 150 nm. This large size is attributed to the interdiffusion of Si at the relatively high growth temperatures employed here, resulting in a decreased lattice mismatch with the substrate (in comparison, QDs grown at lower temperatures, such that the QD composition remains close to pure Ge, have diameters of a few tens of nanometers.^{11,12}

Focused ion beam serial sectioning was performed using an FEI FIB-200 (Ref. 13) with a 30 kV Ga ion beam. The sample was milled using a 70 pA ion beam in serial fashion by positioning the surface of interest parallel to the beam direction and removing material with the edge of the beam. When a flat surface was obtained the sample was rotated 90° such that the newly formed surface was normal to the primary ion beam. The resultant surface was imaged with secondary electrons generated by an 11 pA primary ion beam. This was repeated at 20 nm intervals using an independent reference mark to increment the beam position relative to the surface being milled. This procedure was performed until the total volume of interest was sectioned. The images were processed using Adobe Photoshop (Ref. 14) with the Fovea Pro (Ref. 15) tool kit to increase contrast and, in the case of shape-based interpolation method, to find the edges of quan-

^{a)}Electronic mail: ajk7s@virginia.edu

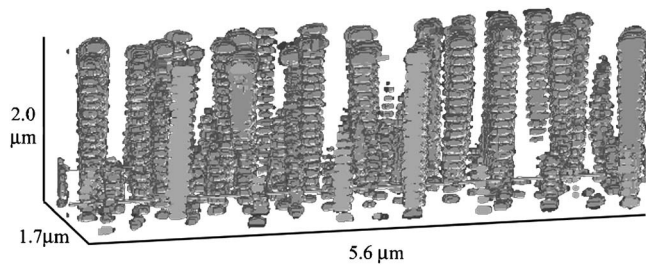


FIG. 1. FIB tomographic reconstruction of the QDs in a Ge/Si quantum dot superlattice. The spatial resolution between the layers was intentionally decreased so that the evolution of the columns could more easily be observed (Ref. 10).

tum dot features. MATLAB (Ref. 16) was used to reconstruct the sectioned volume via a linear interpolation method. Shape-based interpolations were calculated using the computer code developed at the University of Virginia.¹⁷ Figure 1 shows the tomographic reconstruction of the QD superlattice. The serial slices were taken parallel to the front face of the reconstruction and then the volume filled using the shape-based interpolation method. The spatial resolution between QD layers in the original images was intentionally decreased so that the evolution of the columns is more apparent. The flattened faces of some of the QD columns are due to the reconstructed volume intersecting some of the outermost columns.

Upon examination of the tomographic reconstruction in Fig. 1, it can be seen that all of the QD columns in the reconstruction do emanate from the first layer grown and in some cases are extinguished prior to the 20th layer. The termination of QD columns after several layers of growth was predicted by Tersoff *et al.* and Liu *et al.* for QD columns that were too closely spaced.^{3,4} The number density of the QDs on each layer was calculated by viewing cross sections of the reconstructed volume at each layer. Figure 2 is a graph of the number density of QDs on each of the grown layers. The density of QDs on each successive layer decreases until a constant value is reached at the 17th layer. As can be seen in the inset of Fig. 2, the earlier layers consist of a high number density of small QDs while the later layers have a lower density of larger QDs. As some columns disappear, as seen in Fig. 1, the QDs in the other columns increase in size. This

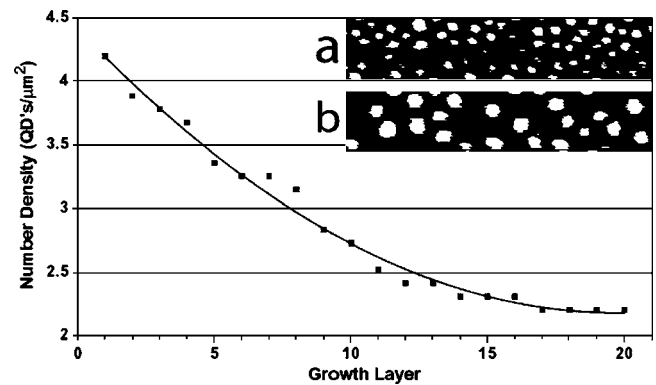


FIG. 2. Number density of QDs as a function of growth layer. Inset (a) is a reconstructed FIB secondary electron image of the first QD layer grown (1) and inset (b) is the last QD layer grown (20).

clearly shows one effect of the three-dimensional self-assembly process.

Another way to examine the three-dimensional ordering of QDs is to plot the size of the QDs on each layer as in Fig. 3. The actual size of the QDs cannot be accurately obtained from these data alone due to both the physical limits of the FIB tomographic technique, i.e., ion and electron interaction volumes, finite beam size, lateral uncertainty in positioning, mixing due to milling, and the postprocessing of the images. These uncertainties combine to produce potential errors of up to 20 nm in the measured feature sizes. For the purpose of this analysis, the sizes of the QDs were normalized to the largest QD base area measured in the system. A curve was drawn connecting the QDs on each individual layer going from the smallest to the largest using the normalized base areas, QD 1 being the smallest QD measured on any given layer. Only the odd numbered QD layers were plotted for the sake of clarity. For the first several layers two trends are observed. The number of QDs on successive layers decreases, and the number of smaller QDs increases. This is the stage where some of the QD columns are terminating, while QDs in other columns increase in size. As columns terminate, the average size of the QDs increases until a final size distribution is reached at around the 17th layer. This is consistent with the constant number density observed in Fig. 2. From TEM images the size distribution of the QDs changed

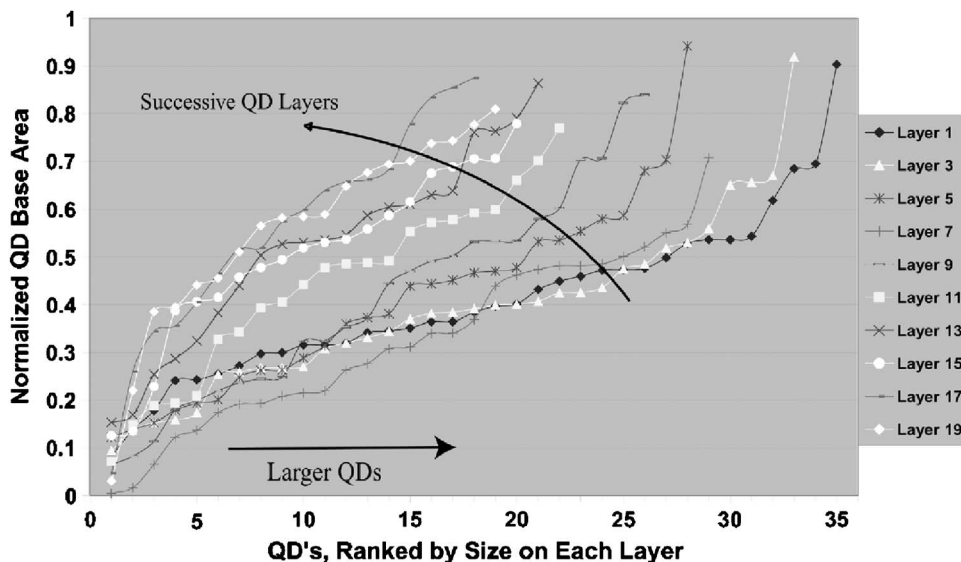


FIG. 3. Normalized area of each QD measured on successive layers. Each line connects the QDs on an individual layer. The normalized QD areas were plotted from smallest to largest, QD 1 being the smallest QD on a given layer. Areas were normalized relative to the largest QD measured in the entire reconstructed superlattice. Only odd numbered layers are displayed to aid in viewing.

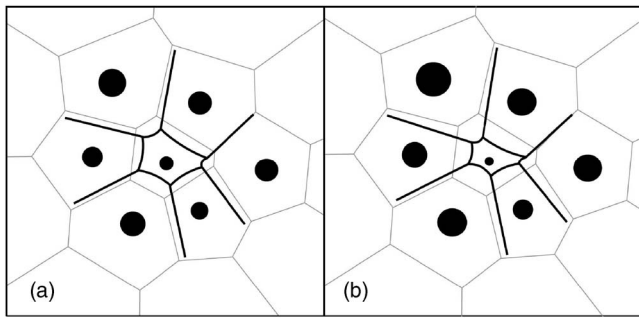


FIG. 4. Comparison of Voronoi polygons (light lines) and compression band network (heavy lines). (a) shows the n th layer of QDs and a schematic illustration of the compression band network on the surface after capping. (b) shows the resulting $(n+1)$ th layer of QDs and the corresponding compression band network after capping.

from being between 120 and 200 nm in diameter on the first layer to between 160 and 220 nm on the final layer. These numbers may be affected by the fact that all observed QDs may not have been completely contained within the thickness of the TEM foil, but the trend in size is confirmed. Since the total amount of Ge deposited on each layer is constant the increase in QD size with a decrease in number density is expected.

If we assume that nucleation of Ge QDs in the first bilayer is essentially random and that the adatom capture region for a QD is purely geometric (which is unlikely given the complex surface diffusion and capture kinetics), we can apply the Voronoi polygon construction.¹⁸ This is done by drawing a locus of points equidistant to the two closest QD centers and terminating it when another locus is intersected. This results in Voronoi polygons each containing one QD. Together the Voronoi polygons fill the two-dimensional space of the QD layer. Each Voronoi polygon has an area that represents the geometrical capture region for surface diffusion by its enclosed QD, and that is proportional to the volume of the enclosed QD. If we assume that: (i) the propagating strain fields from the initial QD layer control nucleation sites on subsequent layers and that (ii) the geometrical capture region, i.e., area of the associated Voronoi polygon, determines the rate of subsequent QD growth, then there would be no spatial reorganization of QDs within the layer and the size distribution of QDs on each layer would remain constant. This is clearly not observed in the current work.

Recent elasticity calculations of surface strain due to buried epitaxial particles with lattice parameters larger than the surrounding matrix show a region in tension directly above the particles. There is also a compressively strained region that, in the case of an isolated particle, forms a ring around the particle if isotropic elasticity is assumed.^{4,19} If multiple particles are embedded, as in the layers of QDs examined here, and they are close enough together, then these compressively strained regions will overlap. A network of compressively strained “bands” would then enclose each QD. If the location of this network is not coincident with the Voronoi polygons (and in general, there is no reason why these networks should coincide) then a strain dependence of surface diffusion would cause QDs to grow at different rates than predicted by simple geometrical capture areas, even for the case of isotropic surface diffusion. Figure 4 illustrates the

change in the adatom capture area for a QD surrounded by other QDs. The light lines show the Voronoi construction while the heavier lines schematically illustrate the compression bands due to strain from the buried QDs. As each successive layer is grown, some of the QD columns increase in diameter while others decrease. The resulting compression band network (CBN) on each successive layer will evolve, such that smaller QD columns will eventually disappear as their associated capture areas in the CBN shrink to zero (Fig. 4). QDs in other columns will grow, until surviving columns are sufficiently separated from each other (i.e., by the operative surface diffusion length before capping commences) such that they do not affect each others growth. A constant configuration is then reached. In this specific experimental case this occurs at about the 17th QD layer.

In summary, we have developed a method for the full three-dimensional characterization of QD superlattices. This enables the relative size and position of all QDs in the system to be individually addressed and compared to the other QDs in the system. We observe that within 20 QD layers the average size increases and the number density decreases to a stable distribution, but the positions of the QDs within the layers are not substantially altered. This is attributed to regions of compressive strain locally modifying surface diffusion.

The authors would like to thank Jerry Tersoff of IBM and Bill Johnson and Steve Policastro of UVa for very insightful discussions. This work was funded by the National Science Foundation Materials Research Science and Engineering Center (MRSEC) on “Nanoscale Materials Design” at the University of Virginia under Award No. DMR-0080016.

¹G. Springholz, M. Pinczolit, V. Holy, S. Zerlauth, I. Vavra, and G. Bauer, *Physica E (Amsterdam)* **9**, 149 (2001).

²V. Le Thanh, V. Yam, Y. Zheng, and D. Bouchier, *Thin Solid Films* **380**, 2 (2000).

³J. Tersoff, C. Teichert, and M. G. Lagally, *Phys. Rev. Lett.* **76**, 1675 (1996).

⁴F. Liu, S. E. Davenport, H. M. Evans, and M. G. Lagally, *Phys. Rev. Lett.* **82**, 2528 (1999).

⁵C. J. Huang, D. Z. Li, B. W. Cheng, J. Z. Yu, and Q. M. Wang, *Appl. Phys. Lett.* **77**, 2852 (2000).

⁶J. Tersoff, *Phys. Rev. B* **43**, 9377 (1991).

⁷A. Madhukar, T. R. Ramachandran, A. Konkar, I. Mukhametzhanov, W. Yu, and P. Chen, *Appl. Surf. Sci.* **123/124**, 266 (1998).

⁸M. A. Lutz, R. M. Feenstra, P. M. Mooney, J. Tersoff, and J. O. Chu, *Surf. Sci.* **316**, L1075 (1994).

⁹R. Hull and J. C. Bean, *Semicond. Semimetals* **56**, 6 (1999).

¹⁰A. J. Kubis, T. E. Vandervelde, J. C. Bean, D. N. Dunn, and R. Hull, *Mater. Res. Soc. Symp. Proc.* **818**, M14.6.1 (2004).

¹¹S. A. Chaparro, J. Drucker, Y. Zhang, D. Chandrasekhar, M. R. McCartney, and D. J. Smith, *Phys. Rev. Lett.* **83**, 1199 (1999).

¹²G. Capellini, M. De Seta, and F. Evangelista, *Appl. Phys. Lett.* **78**, 303 (2001).

¹³FEI Company, Hillsboro, OR 97124.

¹⁴Photoshop, Version 6.0, Adobe Systems Inc., San Jose, CA 95110.

¹⁵Fovea Pro, Reindeer Graphics Inc., Asheville, NC 28801.

¹⁶MATLAB, Version 6.0, The Mathworks Inc., Natick, MA, 01760.

¹⁷D. N. Dunn and R. Hull, *Appl. Phys. Lett.* **75**, 3414 (1999).

¹⁸A. Okabe, B. Boots, K. Sugihara, and S. N. Chiu, *Spatial Tessellations Concepts and Applications of Voronoi Diagrams*, 2nd ed. (Wiley, New York, 2000).

¹⁹S. Policastro and W. C. Johnson (unpublished).